Investigation of the synergistic effect of hydrogen peroxide and ultrasound on the photocatalytic treatment under visible light of dyes wastewater

Domenico Rosa [*], Simona Lattanzio, Irene Bavasso, Luca Di Palma

Department of Chemical Engineering Materials Environment & UdR INSTM, Sapienza-Università di Roma, Via Eudossiana 18, Roma 00184, Italy
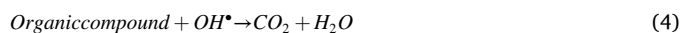
ABSTRACT

A photocatalytic process under visible light irradiation (LED lamp 13 W) assisted by ultrasound and hydrogen peroxide was investigated, aiming at enhancing the hydroxyl radical production compared to simple photo-catalysis. Several parameters, including ultrasound power and H_2O_2 concentration, were investigated in the degradation of Rhodamine B. Fe doped TiO_2 synthesized by the solid-state method was used as the photocatalyst. The synergistic effects between photocatalysis, ultrasound, and H_2O_2 were studied, and the absence of synergy between photocatalysis and ultrasound was demonstrated. Instead, a synergistic effect was observed between photocatalysis and hydrogen peroxide addition, in fact, the combination of photocatalysis with H_2O_2 was demonstrated to totally remove the Rhodamine B (5 ppm) in 2 h, as contaminant removal was greater (by 50 %) when the two treatments were used simultaneously than the removal observed in the individual treatments, attributable to the Fenton reaction that promoted the hydroxyl radicals production.

1. Introduction

Photocatalysis is a very promising technique for the purification of wastewater contaminated by drugs, dyes, and other organic substances that are recalcitrant to the most common treatments. However, the uncontrolled development of human activities and the increasing production of these substances, combined with the increased demand for drinking water, led to the development of new techniques that assist photocatalysis, to reduce operating times and the overall cost of the treatment (Mahendran and Gogate, 2021). The degradation of contaminants occurs, due to the production of hydroxyl radicals (Yegane Badi et al., 2022) (radicals with a high oxidizing power of 2.8 eV (Majeed, 1998) when the catalyst surface is irradiated with light of an appropriate wavelength. The radical's production is due to the formation of a photogenerated positive hole-electron pair when the radiation photo-exciting the electron (the formation of the species responsible for the total mineralization of organic pollutants occurs) according to the following reaction steps (Lingzhiiwangg and Juyingglei, n.d):

$$Semiconductor + hv \rightarrow e_{CB}^- + h_{VB}^+ \qquad (1)$$

$$e_{CB}^- + O_2 \rightarrow O_2^{\bullet-} \qquad (2)$$

$$h_{VB}^+ + H_2O \rightarrow H^+ + OH^\bullet \qquad (3)$$

$$Organic\,compound + OH^\bullet \rightarrow CO_2 + H_2O \qquad (4)$$

Such conditions promote the degradation of highly persistent pollutants to classical treatments. However, because of the adoption of UV light sources, this process is expensive, and the reduction of the operative time can be considered the solution to mitigate this problem that limits the implementation in large-scale applications. In recent years has been paid attention to new methodologies for the synthesis of photocatalysts active under visible light sources (Mahendran and Gogate, 2021). Several Titanium dioxide synthesis methods are reported in the literature, each of them providing a product with a different structure and crystallinity. The preparation method strongly influences the surface characteristics of the photocatalyst. The most widely used synthesis techniques are precipitation, solvothermal method, and sol-gel method (Kuriakose et al., 2013). However, although they have advantages and peculiarities, they require several steps of synthesis and doping, the use of complex and dangerous instrumentation such as autoclaves (Subramaniam et al., 2020) but, more importantly, the use of hazardous reagents (such as nitric acid (Anirudhan et al., 2014) cyclohexane (Lavand et al., 2019).

In any case, the production of waste substances is unavoidable and strategies involving a multi-step approach are used. To avert the production of wastewater (at the doping stage), the "solid-state" method
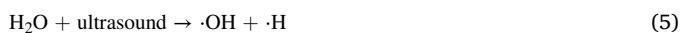
has been employed, which is a simple, inexpensive approach, does not involve the use of hazardous reagents, and is, therefore, free from the problems of the previously mentioned synthesis methods (Rosa et al., 2023a).

Although the high reactivity of such materials has been already proven (Oliveira et al., 2020; Mohan et al., 2021), due to the length required for the treatment, the need of assessing a strategy to comply with high levels of removal requirement in a short time (Litter and Quici, 2010).

It is well known that photocatalysis can be assisted by other processes involving the further production of hydroxyl radicals.

Among such processes, ultrasound appears a promising technique. When a sound wave passes through a fluid, it undergoes a series of expansions and compressions. Such cyclical pressure variations lead molecules to get closer and to step away: if the ultrasounds are sufficiently intense, the vapor pressure of the liquid is exceeded and cavities containing gas are created within the liquid itself (Laborde et al., 1998). The cavitation bubbles undergo oscillation, growth, contraction, and collapse in a very short period, forming a high temperature and high-pressure hot spot around the cavitation nucleus (Yegane Badi et al., 2022) at a temperature of 1900–1500 K and a pressure of 50 MPa (same authors even reported a temperature of 5000 K and a pressure of 100 Mpa (Mahendran and Gogate, 2021). After entering the cavitation bubbles, water molecules decompose to produce highly oxidizing radicals according to the following equations (Monteagudo et al., 2014):

$$H_2O + ultrasound \rightarrow \cdot OH + \cdot H \tag{5}$$

$$\cdot OH + H \cdot \rightarrow H_2O \tag{6}$$

$$H \cdot + O_2 \rightarrow HO_2 \tag{7}$$

$$2HO \cdot \rightarrow H_2O_2 \tag{8}$$

$$2HO_2 \cdot \rightarrow H_2O_2 + O_2 \tag{9}$$

$$H \cdot + H_2O_2 \rightarrow HO \cdot + H_2O \tag{10}$$

In several studies, the addition of hydrogen peroxide was successfully used as a photocatalysis auxiliary method (Yegane Badi et al., 2022; Zuorro et al., 2019): in the presence of light irradiation H_2O_2 undergoes a direct photoscission, thus producing hydroxyl radicals according to the following reactions (Monteagudo et al., 2014; Feilizadeh et al., 2019):

$$H_2O_2 + hv \rightarrow 2HO \tag{11}$$

$$HO \cdot + HO \cdot \rightarrow H_2O_2 \tag{12}$$

$$H_2O_2 + HO \cdot \rightarrow HO_2 \cdot + H_2O \tag{13}$$

$$HO_2 \cdot + HO \cdot \rightarrow H_2O + O_2 \tag{14}$$

$$HO_2 \cdot + HO_2 \cdot \rightarrow H_2O_2 + O_2 \tag{15}$$

Therefore, the present study is concerned with the experimental evaluation of the effect of ultrasound-assisted photocatalysis and hydrogen peroxide with the aim of reducing the cost of applying the process to wastewater treatment (by reducing its operating time), reducing the production of hazardous byproducts (by realizing a reaction environment with greater oxidizing power than photocatalysis alone), and overcoming the limits of applicability for example in a wider pH range (photocatalysis is heavily influenced by this parameter (Lingzhiiwangg and Juyinglei, n.d.).

Titania doped with iron (1 %Fe-TiO$_2$) was used as the photocatalyst (Rosa et al., 2023b), working under visible light irradiation (Mahendran and Gogate, 2021).

Rhodamine B and methylene blue were used as model contaminant to simulate wastewater.

2. Materials and methods

2.1. Chemicals

Titanium diisopropoxide bis-acetylacetonate (75% in isopropanol, Alfa Aesar), ethanol (absolute, >99.8 %, Honeywell), hexahydrate ferric chloride (FeCl$_3$*6H$_2$O, Sigma Aldrich), hydrochloric acid (HCl, 37 %, Honeywell), sulfuric acid (H$_2$SO$_4$, 98 %, Honeywell), Rhodamine B (C$_{28}$H$_{31}$ClN$_2$O$_3$, Carlo Erba), Methylene Blue (MB, C$_{16}$H$_{18}$N$_3$SCl*3H$_2$O, Sigma Aldrich), hydrogen peroxide (H$_2$O$_2$ 30 % Honeywell), *tert*-butyl alcohol (>99.5% Honeywell). All reagents were used without any further purification. Deionized water was used as a solvent for preparing all necessary solutions.

2.2. Photocatalysts synthesis and characterization

The 1 %FeTiO$_2$ catalyst was prepared via "solid-state" method as reported in previous work in which it was also characterized by XRD, SEM, UV–Vis DRS, and BET analysis (Rosa et al., 2023a). An iron load of 1 % was chosen because it has been proved to be the optimal dosage of doping agent on contaminant removal performance.

The 1 %FeTiO$_2$-HCl catalyst was prepared by soaking the 1 %Fe-TiO$_2$ catalyst in a 0.5 M hydrochloric acid solution with a solid-to-liquid ratio of 1:10 for 18 h to leach the surface iron (Zhang et al., 2021). (Fig. 1). UV–vis diffuse reflectance spectroscopy (DRS) using Shimadzu 754 UV–Vis spectrophotometer was employed to determine the light absorption properties of 1 %FeTiO$_2$-HCl nanoparticles. The surface areas, pore sizes, and pore volumes were quantified utilizing the Brunauer-Emmett-Teller (BET) method through N$_2$ adsorption at 77 K using Quantachrome Autosorb-1. To eliminate residual moisture, a preliminary vacuum treatment at 150 °C was administered to the samples prior to measurements.

In addition, the iron content was evaluated by performing Atomic Absorption Spectroscopy (AAS) analysis on the leachate produced by immersing 0.5 g of 1 %Fe-TiO$_2$ and 1 %FeTiO$_2$-HCl samples in a 20 (v/v) % sulfuric acid solution with a solid–liquid ratio of 1:10 for 18 h at 60 °C.

2.3. Photocatalytic evaluation

The experiments were performed in glass bechers (Fig. 2a), filled with 20 ml of Rhodamine B (RB) aqueous solution (5 ppm and 40 ppm) and 20 mg of catalyst (corresponding to the optimal solid–liquid ratio of about 1 g/L (Rosa et al., 2023a). Methylene Blue (MB, 5 ppm) was employed to check the photocatalytic activity. The photocatalyst suspensions were kept under agitation with a mechanical stirrer at a constant rate of 400 rpm (except for ultrasound tests, shown in Fig. 2b). The effect of ultrasound power (ARGO LAB, 30, 50, and 120 W), H$_2$O$_2$ dosage (0.25, 0.50, and 1.00 ml), and irradiance (9 W/m^2, 41 W/m^2, 82 W/m^2) were investigated and the optimal conditions were adopted also for the degradation of Methylene Blue (MB) as a comparative study. The light source adopted was a 13 W LED visible lamp (Osram). Before the activation of light irradiation, the suspension was kept in the dark for 30 min to attain adsorption-desorption equilibrium.

To confirm the effect of hydroxyl radicals on contaminant removal, further tests were carried out by introducing 1 ml of 1 mM *tert*-butyl alcohol (TBA) solution just before activating the lamp.

RB and MB concentrations were determined by UV–vis spectrometry (PG Instruments T8o + UV/Vis spectrophotometer) by measuring the absorbance at 553 nm and 664 nm of the liquid stream separated from the catalyst by centrifugation (10000 rpm for 10 min) At a specific time (0–240 min).

The removal rate was calculated as following:

$$\eta = \frac{A_0 - A(t)}{A_0} * 100 \tag{16}$$

Fig. 1. Materials synthesized: on the left titanium dioxide synthesized (TiO$_2$) according to the procedure given in, in the middle titania doped with 1% of iron according to the "via solid-state" method (1 %Fe-TiO$_2$), on the right 1 %Fe-TiO$_2$ washed with HCl solution 0.5 M for 18 h (1 %FeTiO$_2$-HCl).
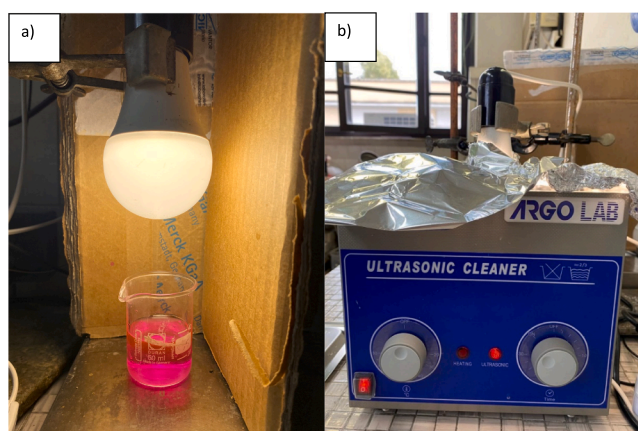

Fig. 2. Experimental setup of (a) photocatalytic tests and (b) photocatalytic tests assisted by ultrasounds.

where η was the pollutant removal efficiency (%), A$_0$ was the pollutant absorbance after the adsorption/desorption equilibrium was achieved and A(t) was the pollutant absorbance of the solution at a selected time t.

3. Results and discussion

3.1. Material characterization

The results of UV–Vis-DRS analysis, the surface area, pore volume and pore size values from the BET analysis were shown in Fig. 3 and in Table 1, respectively.

From Fig. 3, which presents the UV–Vis spectra of the nanoparticles, it is evident that the absorption edge of these samples exhibits a significant shift towards the visible range (1 %Fe-TiO$_2$ and 1 %FeTiO$_2$-HCl samples) in comparison to pure titanium dioxide (TiO$_2$). This phenomenon can be primarily attributed to the incorporation of Fe^{3+} ions within the titanium dioxide's structure, either within interstitial positions or by occupying specific lattice sites of Ti^{4+}.

Furthermore, in the case of the 1 %Fe-TiO$_2$ sample, the presence of a peak between 450 and 500 nm has been observed that can be due to a segregated form of iron, likely hematite (Fe$_2$O$_3$) (Ambrus et al., 2008; Santos et al., 2012); as not all the iron employed for doping was incorporated into the crystalline lattice of titanium dioxide. Indeed, this peak was not observed in samples with lower iron content (0.5 %), as investigated in our previous study (Rosa et al., 2023a). The peak disappeared following the acid treatment to which the sample 1 %FeTiO$_2$-HCl was subjected, an indication that the surface iron oxide was
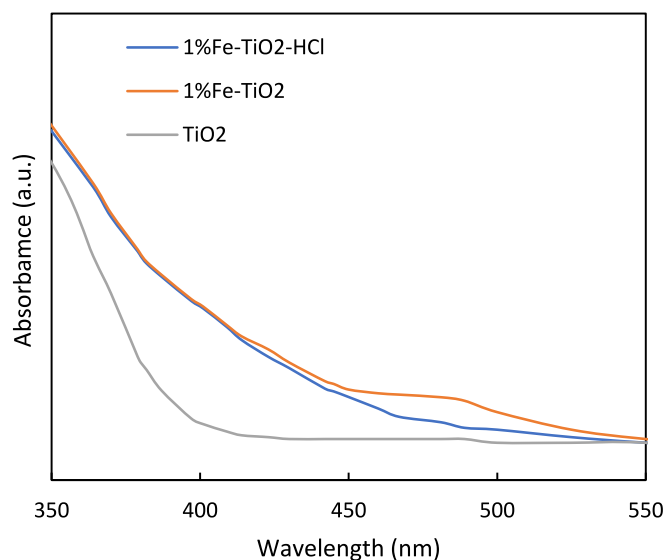

Fig. 3. Diffuse reflectance spectra of titanium dioxide (TiO$_2$), titanium dioxide doped with iron (1 %Fe-TiO$_2$), and titanium dioxide doped with iron and treated with HCl (1 %FeTiO$_2$-HCl).

Table 1
BET analysis: specific surface area (SSA), pore volume, mean pore size of 1 %Fe-TiO$_2$ and 1 %FeTiO$_2$-HCl.

Sample	SSA (m^2/g)	Pore volume (cm^3/g)	Pore size (nm)
1 %Fe-TiO$_2$	10.235	0.031	6.855
1 %FeTiO$_2$-HCl	10.949	0.044	7.124

solubilized.

From the BET analyses, it is evident that all observed surface parameters experienced an increase after the acid treatment. Particularly notable is the augmentation in pore volume. This observation aligns with our previous discussion, suggesting that the segregated iron occluding the pores was solubilized because of the treatment, leading to an enlargement in pore volume.

The leaching tests carried out utilizing sulfuric acid aimed at evaluating the iron content in the samples. The results indicated that the 1 % Fe-TiO$_2$ sample exhibited a solid iron concentration of approximately 9.0 mg/g. In contrast, the 1 %FeTiO$_2$-HCl sample had an iron concentration of 8.1 mg/g. This suggests that approximately 10 % of the iron was solubilized through the hydrochloric acid treatment, revealing its

presence as an aggregate on the catalyst surface.

3.2. Photocatalytic degradation: Irradiance effect and kinetic study

In our previous study, the pivotal role of Irradiance was pointed out, and, also in the case of RB photodegradation, the effect of different Irradiance energies in the range 0–82 W/m^2 was investigated (Rosa et al., 2023a). The optimal conditions found in our previous study were adopted in the present work: pH = 7, catalyst dosage = 1 g/L, iron content = 1 %. The results of RB degradation are reported in Fig. 4 at two different RB initial concentrations (5 ppm in Fig. 4a and 40 ppm in Fig. 4c). Data show that for the 5 ppm RB solution, after 4 h a degradation of 90 % under visible light irradiation of 82 W/m^2 was observed, compared to the 5 % removal recorded when no-light is applied and when adsorption is the only mechanism for RB removal. The strong enhancement in RB removal observed under irradiation was due to the increased production of positive hole-electron pairs caused by light energy and the resulting increase in hydroxyl radicals production (Li et al., 2008).

Fig. 4c shows that the lower removal was observed for the highly concentrated solution (40 ppm): the darker color of the solution due to the higher organic content affected photon penetration into the liquid bulk to reach the catalyst surface (Lingzhiiwangg and Juyingglei, n.d).

A comparison between RB and MB was then performed. Fig. 4d shows that the same behavior was observed for both contaminants, but the removal rate of MB dye was higher than that of RB dye, due to their different chemical structures, which resulted in differences in both adsorption properties and susceptibility to photodegradation (the more complex chemical structure of RB makes it less photodegradable). In addition, the absorption of light photons by the dye leads to fewer photons being available for hydroxyl radical generation. In fact, RB strongly absorbs visible radiation ([RB] = 5 ppm: Absorbance = 1.30 at λ_{max} = 554 nm) compared to MB ([MB] = 5 mg/l: Absorbance = 1.10 at λ_{max} = 664 nm), leading to a lower photodegradation. The strong adsorption of light by the dye molecules is believed to have an inhibitory effect on the photogeneration of holes or hydroxyl radicals, due to the lack of direct contact between the photons and the photocatalyst. Dye molecules adsorb light, and the photons do not reach the surface of the photocatalyst, thus reducing the efficiency of photodegradation. Moreover, the adsorption of the target molecule onto the nanoparticle surface is a critical step toward efficient photocatalysis. Tests performed to evaluate the adsorption rate showed that, for a 5 mg/l solution, at equilibrium conditions, removal of RB was 5 % (Fig. 4a) while for MB 15 % was achieved. Since hydroxyl radicals have very short half-lives, about 70 ns, so they can react only near the surface of the catalyst: according to the Einstein-Smoluchowski equation given below:

$$\Delta X = \sqrt{2Dt} \tag{17}$$

with D = 2.3 × 10^{-5} cm^{2}s^{-1} for hydroxyl radicals, so they can only diffuse through an average distance of 180 Å. A side reaction may also occur between the hydroxyl radical and the hydrogen atoms of the side chains. This reaction competes with the destruction of the chromophore of the dye, without leading to a decrease in the absorbance of the solution (Hashemzadeh et al., 2013).

A pseudo-first order kinetic was observed, which accurately represented the data (Fig. 4b), in agreement with other literature studies (Wei et al., 2018; Yu et al., 2009; Khasawneh et al., 2021), according to the equation:

$$\ln\left(\frac{c_0}{c_t}\right) = kt \tag{18}$$

where C_t is the actual concentration at different times, C_0 is the concentration at time 0 (measured after 30 min of stirring in dark conditions), and k is the kinetic constant (min^{-1}).

Table 2
Kinetic constant and R^2 values for the photocatalytic degradation of RB (C$_0$ = 5 ppm) at different Irradiance values.

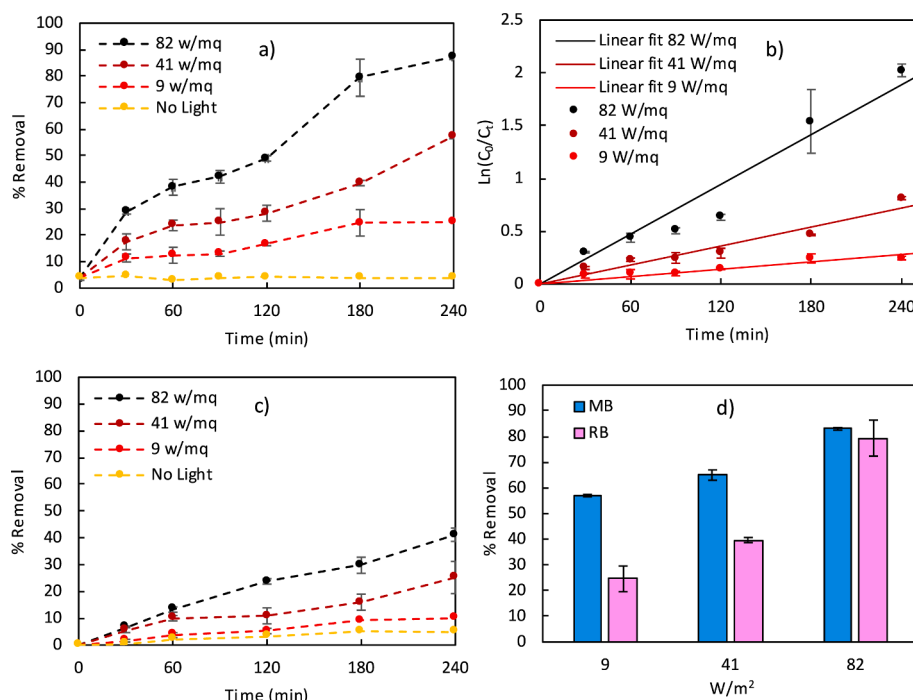| Irradiance (W/m^2)	k (min^{-1})	R^2
9	0.0012±0.0001	0.959±0.012
41	0.0030±0.0001	0.974±0.009
82	0.0079±0.0006	0.971±0.010

Fig. 4. % Removal of RB at an initial concentration of 5 ppm (a) and their kinetic study (b) and 40 ppm (c), at different irradiance values. d) Comparison between RB and MB, both at an initial concentration of 5 ppm, 1 g/L of the catalyst (1 %Fe-TiO$_2$) at different irradiance values after 180 min.

Table 2 shows the kinetics constants (k) of photochemical degradation obtained from Eq. (18) (Yegane Badi et al., 2022; Hashemzadeh et al., 2013).

A linear correlation was then found between irradiation and kinetic constant: in the investigated range (9–82 W/m^2) the formation electron-positive hole was predominant while their recombination was negligible for both RB and MB, as shown in Fig. 5.

A linear correlation between light source and reaction rate was observed, although the kinetic k values are lower than those reported in other works (Li et al., 2008).

Nadir Abbas et al. (2016) (Abbas et al., 2016) by employing an iron-doped titania catalyst synthesized by the sol-gel method and a 100 W Halogen Lamp light source with an irradiance of 850 W/m^2 obtained a first order k = 0.0162 (min^{-1}), almost double the value of the k reported in this work.

Youji et al. (2008) (Hashemzadeh et al., 2013) also reported in their work a kinetic constant k = 0.017 (min^{-1}) employing a titania-based catalyst supported with activated carbon (AC/TiO$_2$) and by using a UV lamp with an irradiance of 250 W/m^2 as the light source.

This difference can be attributed to the use, in the present study, of a lower irradiance light source so it is reasonable to assume due to the linearity relationship between Irradiance and k kinetics that the 1 %Fe-TiO$_2$ catalyst could have performance comparable to that of the catalysts mentioned above.

3.3. Assisted photocatalysis tests

The results of tests of US-assisted photocatalysis, H$_2$O$_2$, and a combination of US and H$_2$O$_2$ are below reported.

3.3.1. Ultrasound-assisted

To assess the interaction between photocatalysis and ultrasound, ultrasonic tests were carried out both with and without hydroxyl radical scavenger (1 ml of 1 mM TBA solution), as illustrated in Fig. 6a. It was observed that ultrasound treatment alone (at 120 W) removed approximately 9% of the contaminant after 30 min of treatment. The removal rate exhibited a slight increase with time; indeed, after 180 min, the removal rate reached 12 %. The introduction of the scavenger led to a drastic reduction in removal efficiency (4 % after 180 min), implying

that the observed decolorization was primarily attributed to the production of hydroxyl radicals by ultrasound, as represented by Equation (5).

The effect of ultrasound at different power was also evaluated. From Fig. 6b is possible to observe that the removal rate was enhanced by increasing US power. However, at the lowest powers adopted (35 and 50 W), a lower removal rate is observed with respect to the tests carried out only with photocatalysis under the same conditions (25 % after 90 min). This could be attributed to inadequate agitation: US tests were in fact carried out in the ultrasonic bath, without using a magnetic stirrer (as generally in photocatalytic tests occurs). To investigate the stirring effect, tests were carried out with the sonicator off, showing a significant decrease in the removal percentage. With an initial concentration of RB 5 ppm and Irradiance 41 w/m^2, only a 5 % removal was achieved, compared with 24 % removal obtained at the same conditions but under continuous stirring. Conversely, at an irradiance of 120 W, a significant improvement in contaminant removal was observed, becoming more pronounced as the treatment duration increased. Specifically, after 30 min of ultrasonic treatment, a difference of approximately 1 % was noted, while after 180 min, this difference increased to around 10 % (Fig. 6c). This phenomenon could be due to reduced nanoparticle aggregation, as corroborated by Dynamic Light Scattering (DLS) analyses. Notably, the DLS results revealed a decrease in nanoparticle aggregation due to ultrasonic treatment. Initial hydrodynamic diameter measurements of 160 nm decreased to 100 nm after 30 min of exposure to 120 W ultrasonic power, and further reduced to 60 nm after 180 min. As a result, US 120 W was then used to assist photocatalysis.

Tests carried out with US 120 W showed that ultrasounds contributed to contaminant removal through the production of hydroxyl radicals produced by water decomposition (Mahendran and Gogate, 2021; Monteagudo et al., 2014). The same tests were performed on MB and the same behavior was observed (Fig. 6d).

3.3.2. Hydrogen peroxide addition assisted

Experimental tests were performed with different amounts of H$_2$O$_2$ 30 v/v% to evaluate the optimal dosage: the results are reported in Fig. 7.

An increase in dye removal at increasing hydrogen peroxide dosage was observed, due to hydrogen peroxide oxidizing effect onto the
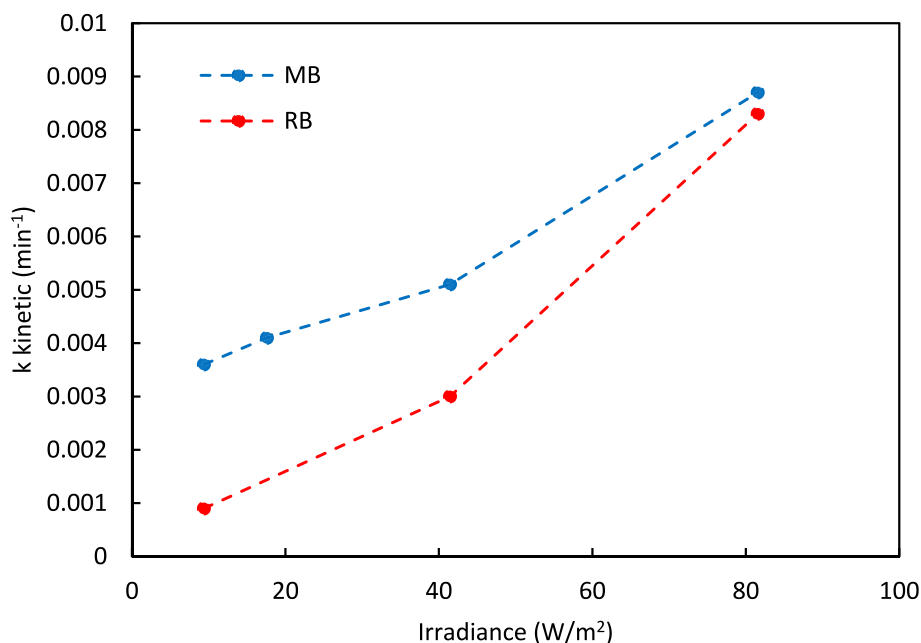

Fig. 5. Kinetics constant (k) as a function of irradiance for MB and RB (C$_0$ = 5 ppm): tests performed at 1 g/L of catalyst (1 %Fe-TiO$_2$), and with an Osram LED lamp of 13 W.
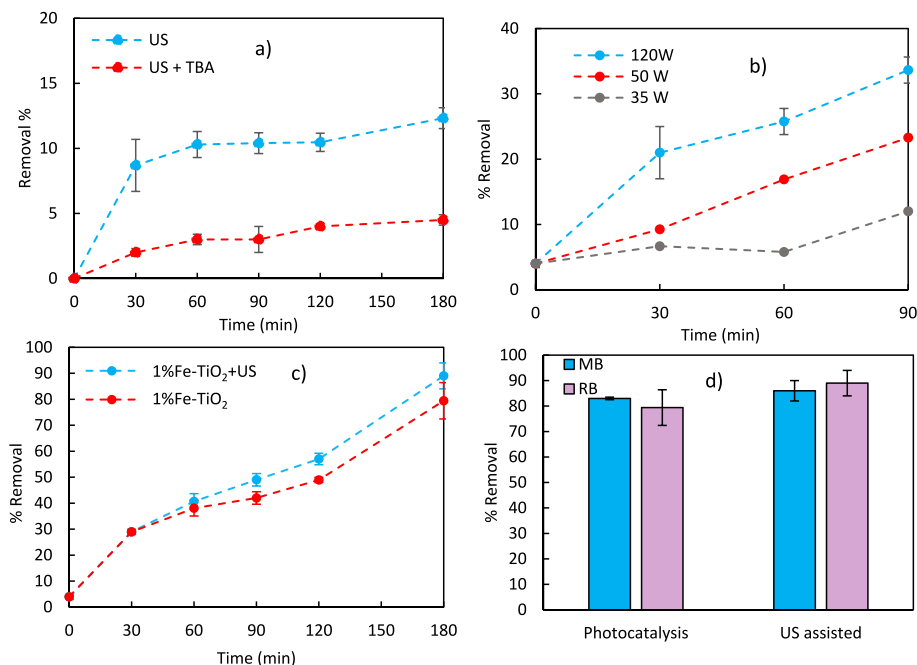
Fig. 6. a) Hydroxyl radical production verification, irradiance 41 W/m^2, RB 5 ppm, US 120 W (without catalyst), and 1 ml of 1 mM TBA added. % Removal of RB 5 ppm using 1 g/L of catalyst (1 %Fe-TiO$_2$), b) Irradiance 41 W/m^2, c) Irradiance 82 W/m^2 using US 120 W and the same conditions without US, d) US 120 W effect: comparison between RB and MB (Irradiance 82 W/m^2 after 180 min).
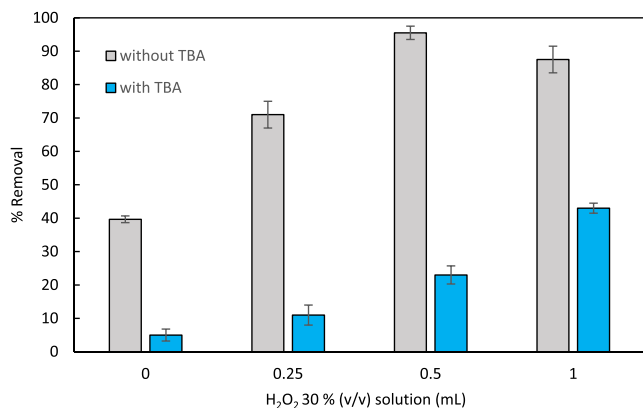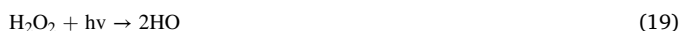

Fig. 7. % Removal of RB at the initial concentration of 5 ppm using 1 g/L of catalyst (1% Fe-TiO$_2$) at irradiance 41 W/m^2 after 120 min on volume solution of 20 ml without and with 1 ml of 1 mM TBA solution addition.

organic contaminant, by producing hydroxyl radicals through decomposition (Eq. (19)) (Feilizadeh et al., 2019).

$$H_2O_2 + hv \rightarrow 2HO \tag{19}$$

Another significant factor to consider in hydroxyl radical production is the Fenton effect. This is a recognized advanced oxidation process wherein iron-based semiconductors like Fe$_2$O$_3$ are employed (S. H U -S U N G L I N and A N D M I R A, 1998). In the presence of hydrogen peroxide and a light source, these semiconductors generate hydroxyl radicals, which are valuable for decontaminating organic substances (Thomas et al., 2021).

The general mechanism of the Fenton process can be represented as follows:

$$Fe^{2+} + H_2O_2 \rightarrow Fe^{3+} + \cdot OH + OH^- \tag{20}$$

$$Fe^{3+} + H_2O_2 \rightarrow Fe^{2+} + \cdot OOH + H^+ \tag{21}$$

Hydrogen peroxide reacts with Fe^{2+} to generate hydroxyl radicals. However, the production of Fe^{2+} poses a challenge due to the inherently slow kinetics of the reduction of Fe^{3+} to Fe^{2+} (Wang, 2008). Consequently, various studies suggest that the utilization of light energy (Feng et al., 2006) could offer an advantageous and cost-effective alternative to expedite the regeneration of Fe^{2+} in the Fenton reaction (Rubio et al., 2013). A heterogeneous Fenton system can generate hydroxyl radicals through two distinct pathways. It can involve a genuine heterogeneous catalytic mechanism or a homogeneous Fenton reaction that occurs due to iron leaching from the solid catalyst (He et al., 2017), in any scenario, this process can be utilized in conjunction with photocatalysis.

To confirm this catalyst-free mechanism, additional tests were carried out with scavenger addition and with and without light radiation: significant contaminant removal was observed in both cases, thus confirming the oxidizing capability of hydrogen peroxide. However, in the presence of light radiation, a higher removal efficiency was obtained, due to hydrogen peroxide faster degradation under light radiation. The addition of the hydroxyl radical scavenger markedly diminished the contaminant removal, thereby confirming that a significant portion of the degradation is indeed attributed to the hydroxyl radicals formed from hydrogen peroxide.

Conversely, hydrogen peroxide could also act as a scavenger of hydroxyl radicals thus reducing their availability in decomposing the organic contaminant (Lingzhiiwangg and Juyingglei, n.d.; Monteagudo et al., 2014; Feilizadeh et al., 2019). Another radical species less reactive than hydroxyl radical is in fact formed, the hydroxyperoxyl radical HO$_2\cdot$ (E^0 = 1.7 vs 2.8 V) (Litter and Quici, 2010).

To prevent this drawback, the following photocatalysis-assisted tests were performed with the addition of hydrogen peroxide at the optimal dosage (0.5 ml per 20 ml of solution). The results of such tests are shown in Fig. 8a and b.

It is evident from Fig. 8 that the addition of hydrogen peroxide brings a significant improvement in contaminant removal compared to photocatalysis alone, due to above mentioned increased production of hydroxyl radicals (Feilizadeh et al., 2019). Complete removal was achieved within 3 h (41 W/m^2). Higher irradiance conditions greatly enhanced the removal kinetics (Majeed, 1998): in fact, in only 2 h a
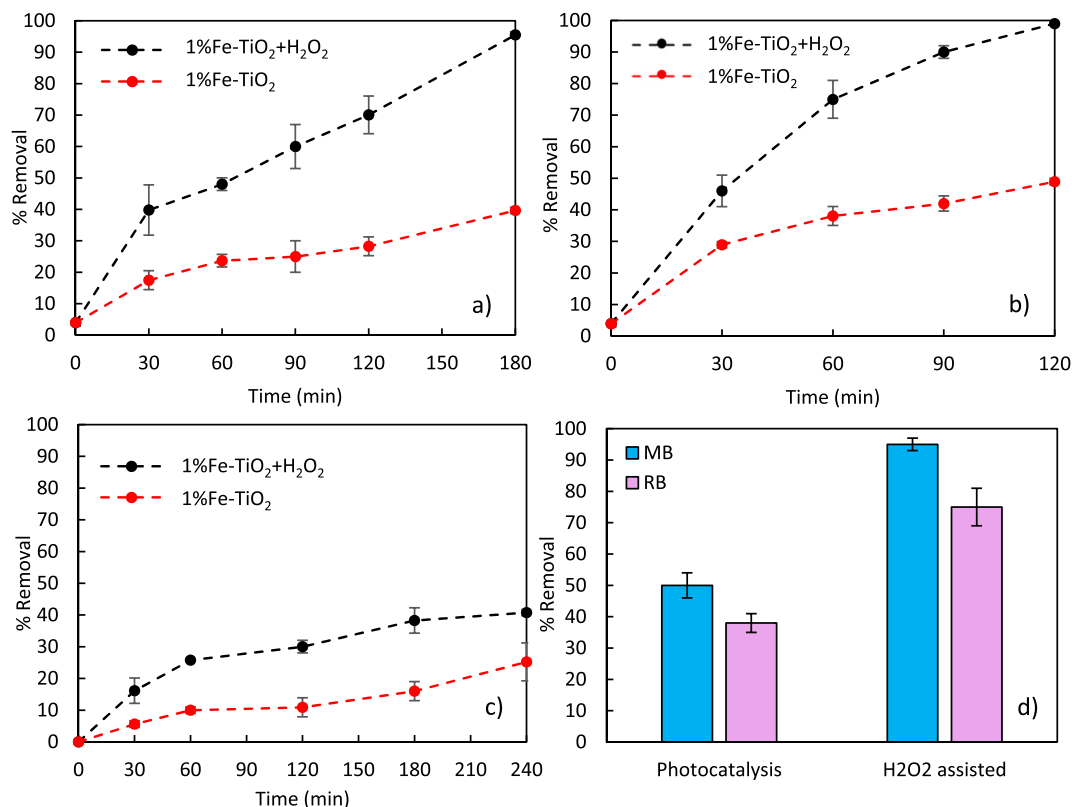
Fig. 8. Effect of hydrogen peroxide addition (dose: 0.5 ml H_2O_2 30 % v/v per 20 ml solution): RB removal at the initial concentration of 5 ppm, 1 g/L of catalyst (1% Fe-TiO$_2$). a) irradiance value of 41 W/m^2. b) Irradiance 82 W/m^2. c) RB removal at the initial concentration of 40 ppm, irradiance value 41 W/m^2. d) Comparison between MB and RB at irradiance value 82 W/m^2 after 60 min.

complete removal of the contaminant was obtained, at an irradiance of 82 W/m^2.

Tests performed at a higher contaminant concentration (40 mg/l) showed the same beneficial effect by hydrogen peroxide addition, as shown in Fig. 8c.

In this case, complete removal of the contaminant is not achieved in the 240 h test, and longer times of treatment are required. The same behavior was also shown by tests performed with MB, as shown in Fig. 8d, where the removal efficiency of the two selected dyes is compared at the same experimental conditions.

In agreement with the above reported results, MB showed higher removal rates than RB.

3.3.3. Photocatalysis assisted by US and H_2O_2

Tests of ultrasound-assisted photocatalysis with hydrogen peroxide addition under the optimal conditions discussed above were then carried out. It can be seen from Fig. 9 how the simultaneous combination of the two techniques further reduces (to 1 h only) the time to achieve a complete contaminant removal.

Treatment efficiency in a pH range of 3–10 was tested, (the pH was adjusted by the addition of appropriate amounts of NaOH or HCl solution), showing promising results; in fact, almost complete removal of the contaminant in the investigated range was observed after 1 h in a wide range of pH (Fig. 10).

This is an important result that showed that such treatment is not affected by pH but worked in the whole investigated pH range (3–10) as opposed to what obtained by some where pH values have been shown to heavily affect the performance of the catalyst and the whole treatment (Dariani et al., 2016; Uddin et al., 2012; Monteagudo et al., 2014). This can be explained by a combination of different effects that contribute to contaminant removal. At alkaline pHs, the degradation of both the added H_2O_2 and the H_2O_2 produced by US is favored, according to Eqs. (8) and (9), (Meng et al., 2022) so there is increased production of hydroxyl radicals responsible for contaminant degradation. In addition,
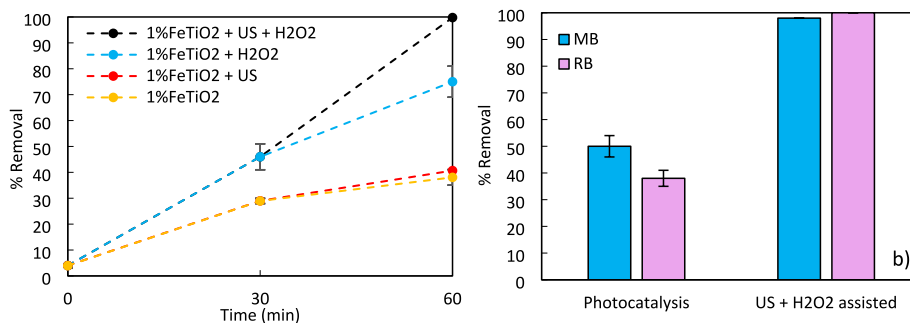

Fig. 9. A) Effect of US and H_2O_2 combine with photocatalysis: Removal of RB (C_0 = 5 ppm): tests performed at 1 g/L of catalyst (1% Fe-TiO$_2$), irradiance value = 82 w/m^2, US = 120 W, and H_2O_2 30 % v/v solution 0.5 ml/20 ml solution. b) Comparison between RB and MB after 60 min of treatment.
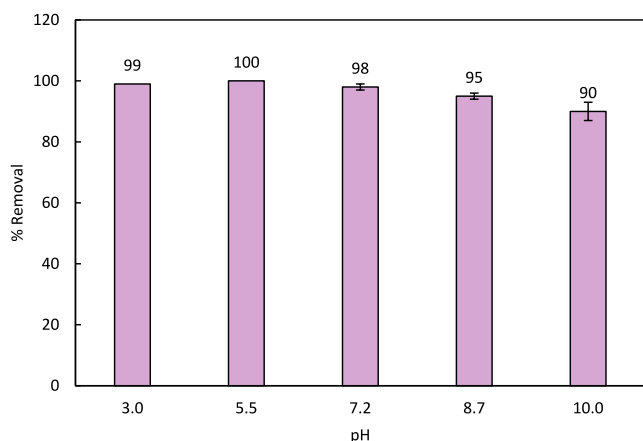
Fig. 10. Effect of pH on the Removal of RB ($C_0 = 5$ ppm): tests performed at 1 g/L of catalyst (1% Fe-TiO$_2$), irradiance value = 82 w/m^2, US = 120 W, and H$_2$O$_2$ 30 % v/v solution 0.5 ml/20 ml solution for 60 min.

under acidic conditions, Fenton reaction between iron and H$_2$O$_2$ is favored (Merouani et al., 2022); allowing hydroxyl radical production according to Eq. (20). Since contaminant removal depends on the nature of the contaminant and the interaction with the catalyst surface, another important effect is related to the electrostatic interaction between RB and the catalyst. At pH higher than 4.1, RB possesses a deprotonated carboxylic group, negatively charged, while a positive surface charge is observed on the catalyst surface at pH below 7.3 (zero charge pH measured for the 1 %Fe-TiO$_2$ catalyst). Consequently, in the pH range between 4 and 7, the electrostatic interaction is strongly enhanced, thus allowing better adsorption of the contaminant, and favoring the reaction with radicals near the catalyst surface (Chen et al., 2003).

A comparison was also made with the other selected contaminant

(Methylene Blue, MB) at the natural pH of the solution (pH 7), (Fig. 9b): the same behavior was observed, although, as expected, rhodamine B was more difficult to degrade given the greater chemical complexity of the molecule (Hashemzadeh et al., 2013).

3.4. Synergistic effect study on photocatalysis assisted with US and H$_2$O$_2$

To evaluate the synergy between photocatalysis, US, and hydrogen peroxide, tests were carried out using hydrogen peroxide only, US only (in the absence of catalyst), and photocatalysis tests. These last tests were carried out with a 1 %FeTiO$_2$-HCl catalyst (suitably treated to remove surface Fe) both alone and assisted with H$_2$O$_2$ addition. The results are shown in Fig. 11.

From Fig. 11, it was possible to observe that hydrogen peroxide alone had an oxidizing power in agreement with Eq. (19) responsible for the degradation of the contaminant due to the formation of hydroxyl radicals obtained by the decomposition of hydrogen peroxide. The 1 %Fe-TiO$_2$ and 1 %FeTiO$_2$-HCl photocatalysts also showed contaminant removal capacity but by adding hydrogen peroxide the removal increased significantly, the effect was more pronounced for the 1 %Fe-TiO$_2$ catalyst and less for 1 %FeTiO$_2$-HCl, therefore, it was not possible to attribute the large increase in contaminant removal rate to hydrogen peroxide degradation alone otherwise the same benefit should have been observed for both catalysts. An attempt was therefore made to understand the reason for this difference; experimental data reported in Fig. 11 were then processed by plotting the synergy factor (S) as a function of time in Fig. 12. S was defined as the removal rate of the combined treatments versus the summation of the removal rate of the individual treatments according to the equation below (Yegane Badi et al., 2022; Fernandes et al., 2020).

$$S = \frac{\%Removal(Combinate\,treatment)}{\sum \%Removal(Single\,treatment)} \tag{22}$$

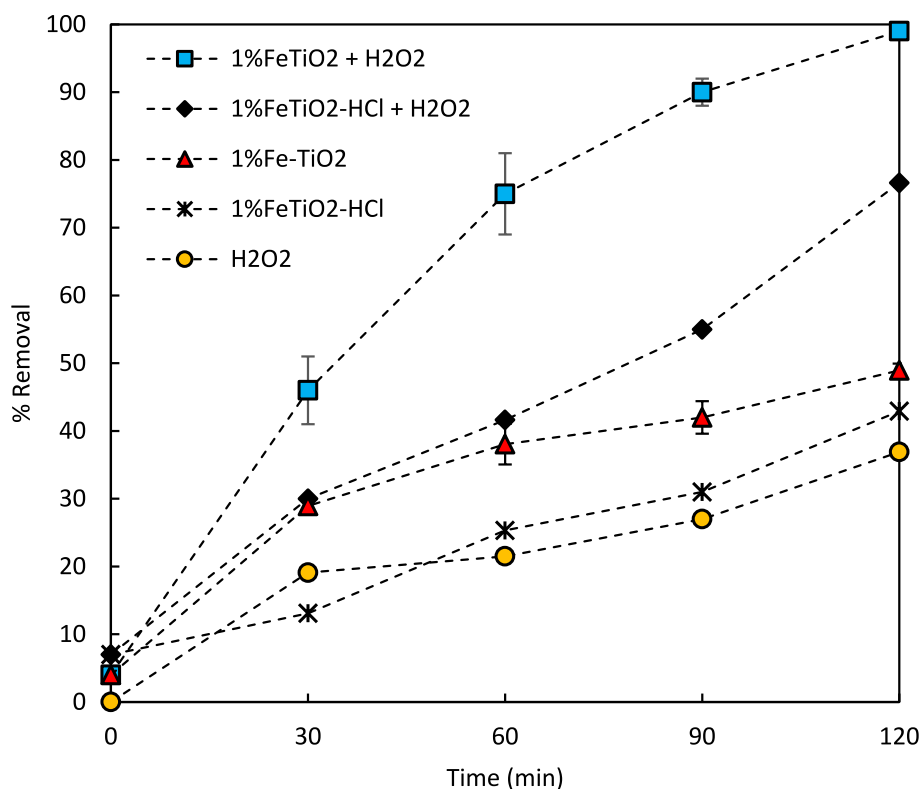According to this definition (Eq. (22)), when S is <1, the degradation

Fig. 11. Removal of RB ($C_0 = 5$ ppm): tests performed at 1 g/L of the catalyst (1% Fe-TiO$_2$ and 1 %FeTiO$_2$-HCl), irradiance value = 82 w/m^2, H$_2$O$_2$ 30 % v/v solution 0.5 ml/20 ml.
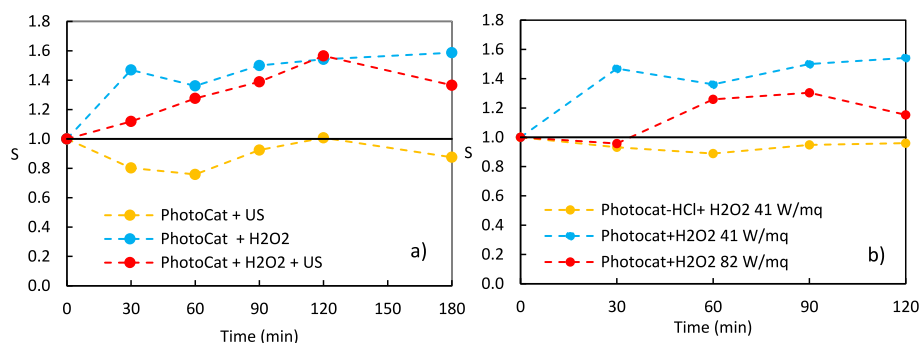
Fig. 12. Synergy factor (S) as a function of the time: Removal of RB ($C_0 = 5$ ppm) (a) using 1 g/L of the catalyst (1 %Fe-TiO$_2$) at irradiance value 41 w/m^2, H$_2$O$_2$ 0.5 ml/20 ml, US 120 W, b) using 1 g/L of the catalyst (1 %Fe-TiO$_2$ and 1 %FeTiO$_2$-HCl) at irradiance value 41 w/m^2, H$_2$O$_2$ 0.5 ml/20 ml.

rate of the combined process is lower than the sum of the processes considered individually, which means that there is no advantage in using the two treatments simultaneously but is even disadvantageous as they may conflict with each other. When if S is about 1 it means that there is no synergistic effect between the two treatments. When S is >1 a positive synergistic effect between the treatments considered is observed.

Fig. 12a shows that no positive synergy in using photocatalysis and ultrasound simultaneously occurred, (S is always <1), since photocatalysis and ultrasound act as sources of hydroxyl radical production independently of each other. At the beginning of the tests, a worsening attributable to a diffusion problem is even noticed since the tests performed with the US were carried out in the US bath without magnetic stirring. The addition of H$_2$O$_2$ to photocatalysis achieved about 60 % more benefit in contaminant degradation that did not occur when photocatalysis and hydrogen peroxide are separately tested (Yegane Badi et al., 2022).

Fig. 12b shows that using the 1 %FeTiO$_2$-HCl catalyst washed with hydrochloric acid (and, therefore, without iron on the catalyst surface), the synergistic effect due to the addition of hydrogen peroxide was completely nullified. This means that the observed synergism is due to the iron on the catalyst surface, that, according to the analysis performed on the leachate by atomic absorption spectrophotometer (AAS), accounted about to the 10 % of the total iron employed for doping. In fact, in the absence of surface iron, the catalyst and hydrogen peroxide acted as a source of hydroxyl radicals independently of each other. It is also interesting to notice that as the irradiance increased, the positive synergistic effect decreased, probably because photocatalysis tends to override all other effects that contribute to contaminant degradation and are not dependent on the irradiance employed.

The increased production of hydroxyl radicals by surface iron and hydrogen peroxide could be explained through the heterogeneous photo Fenton effect (Dariani et al., 2016).

4. Conclusions

In this work, the optimal conditions were found to assist photocatalysis with ultrasound and the addition of hydrogen peroxide by employing a simple-to-synthesize and inexpensive catalyst capable of working under visible light. It was demonstrated that the use of US, H$_2$O$_2$, and catalysts can remove the tested contaminants (RB and MB 5 ppm) within 60 min of treatment.

Hydrogen peroxide and US-assisted photocatalysis effectiveness was slightly affected by pH in the explored range (from 3 to 10); in fact, despite the maximum contaminant removal efficiency was observed at pH 5.5, satisfactory removal rates (>90 %) were obtained in the whole investigated range (pH 3–10). Synergistic effects were also studied demonstrating how there is no positive synergy between photocatalysis and ultrasound and better clarifying the nature of the significant synergism between catalyst and hydrogen peroxide addition.

The linear dependence between the kinetic constant of the reaction and the irradiance employed was also demonstrated, thus being able to affirm the competitiveness of the material compared to other works where they employ different light sources.

Future developments will be aimed at testing the catalyst on other contaminants and more chemically complex solutions while also investigating its reusability.

Declaration of Competing Interest

The authors declare that they have no known competing financial interests or personal relationships that could have appeared to influence the work reported in this paper.

Data availability

Data will be made available on request.

References

Abbas, N., Shao, G.N., Haider, M.S., Imran, S.M., Park, S.S., Kim, H.T., 2016. Sol–gel synthesis of TiO2-Fe2O3 systems: Effects of Fe2O3 content and their photocatalytic properties. Journal of Industrial and Engineering Chemistry 39, 112–120. https://doi.org/10.1016/j.jiec.2016.05.015.

Ambrus, Z., Balázs, N., Alapi, T., Wittmann, G., Sipos, P., Dombi, A., Mogyorósi, K., 2008. Synthesis, structure and photocatalytic properties of Fe(III)-doped TiO2 prepared from TiCl3. Applied Catalysis. B, Environmental 81 (1-2), 27–37.

Anirudhan, T.S., Divya, P.L., Nima, J., Sandeep, S., 2014. Synthesis and evaluation of Iron-doped titania/silane based hydrogel for the adsorptional photocatalytic degradation of Victoria blue under visible light. Journal of Colloid and Interface Science 434, 48–58. https://doi.org/10.1016/j.jcis.2014.07.030.

F. Chen, J. Zhao, and H. Hidaka, "Highly selective deethylation of rhodamine B: Adsorption and photooxidation pathways of the dye on the TiO 2/SiO 2 composite photocatalyst," 2003.

Dariani, R.S., Esmaeili, A., Mortezaali, A., Dehghanpour, S., 2016. Photocatalytic reaction and degradation of methylene blue on TiO2 nano-sized particles. Optik (Stuttg) 127 (18), 7143–7154. https://doi.org/10.1016/j.ijleo.2016.04.026.

Feilizadeh, M., Attar, F., Mahinpey, N., 2019. Hydrogen peroxide-assisted photocatalysis under solar light irradiation: Interpretation of interaction effects between an active photocatalyst and H2O2. Canadian Journal of Chemical Engineering 97 (7), 2009–2014. https://doi.org/10.1002/cjce.23455.

Feng, J., Hu, X., Yue, P.L., 2006. Effect of initial solution pH on the degradation of Orange II using clay-based Fe nanocomposites as heterogeneous photo-Fenton catalyst. Water Research 40 (4), 641–646. https://doi.org/10.1016/j.watres.2005.12.021.

Fernandes, A., Makoś, P., Wang, Z., Boczkaj, G., 2020. Synergistic effect of TiO2 photocatalytic advanced oxidation processes in the treatment of refinery effluents. Chemical Engineering Journal 391, 123488.

F. Hashemzadeh, R. Rahimi, A. Ghaffarinejad, F. Hashemzadeh, R. Rahimi, and A. Gaffarinejad, "Photocatalytic Degradation of Methylene blue and Rhodamine B dyes by Niobium Oxide Nanoparticles synthesized Via Hydrothermal method," Online, 2013. [Online]. Available: http://www.ijacsr.com/.

He, D., Chen, Y., Situ, Y., Zhong, L., Huang, H., 2017. Synthesis of ternary g-C 3 N 4/Ag/γ-FeOOH photocatalyst: An integrated heterogeneous Fenton-like system for effectively degradation of azo dye methyl orange under visible light. Applied Surface Science 425, 862–872. https://doi.org/10.1016/j.apsusc.2017.06.124.

Khasawneh, O.F.S., Palaniandy, P., Ahmadipour, M., Mohammadi, H., Bin Hamdan, M. R., 2021. Removal of acetaminophen using Fe2O3-TiO2 nanocomposites by

photocatalysis under simulated solar irradiation: Optimization study. Journal of Environmental Chemical Engineering 9 (1), 104921.

Kuriakose, S., Bhardwaj, N., Singh, J., Satpati, B., Mohapatra, S., 2013. Structural, optical and photocatalytic properties of flower-like ZnO nanostructures prepared by a facile wet chemical method. Beilstein Journal of Nanotechnology 4 (1), 763–770. https://doi.org/10.3762/bjnano.4.87.

Laborde, J.-L., Bouyer, C., Caltagirone, J.-P., Gérard, A., 1998. Acoustic bubble cavitation at low frequencies. Ultrasonics 36 (1-5), 589–594.

Lavand, A.B., Bhatu, M.N., Malghe, Y.S., 2019. Visible light photocatalytic degradation of malachite green using modified titania. Journal of Materials Research and Technology 8 (1), 299–308. https://doi.org/10.1016/j.jmrt.2017.05.019.

Li, Y., Sun, S., Ma, M., Ouyang, Y., Yan, W., 2008. Kinetic study and model of the photocatalytic degradation of rhodamine B (RhB) by a TiO2-coated activated carbon catalyst: Effects of initial RhB content, light intensity and TiO2 content in the catalyst. Chemical Engineering Journal 142 (2), 147–155. https://doi.org/10.1016/j.cej.2008.01.009.

J. B. Lingzhiiwangg· and M. Juyingglei, "Lecture Notes in Chemistry 100 Photocatalysis Fundamentals, Materials and Applications." [Online]. Available: http://www.springer.com/series/632.

M. I. Litter and N. Quici, "Photochemical Advanced Oxidation Processes for Water and Wastewater Treatment." 2010.

Mahendran, V., Gogate, P.R., 2021. Degradation of Acid Scarlet 3R dye using oxidation strategies involving photocatalysis based on Fe doped TiO2 photocatalyst, ultrasound and hydrogen peroxide. Separation and Purification Technology 274, 119011.

L. Majeed and A. al Rihaymee. "Enhanced Photocatalytic Activity of Titanium Dioxide Nanoparticles by Metal Deposition." 1998.

Meng, L., Chang, L., Hou, J., 2022. Degradation of methyl green from wastewater with ultrasound synergized with Bi2O2CO3 catalysis: Kinetics, products, and pathways. Journal of Cleaner Production 342, 130976.

Merouani, S., Dehane, A., Belghit, A., Hamdaoui, O., el Houda Boussalem, N., Daif, H., 2022. " Removal of persistent textile dyes from wastewater by Fe(ii)/H 2 O 2/H 3 NOH + integrated system: process performance and limitations", Environmental Science. Advances 1 (2), 192–207. https://doi.org/10.1039/d2va00011c.

Mohan, H., Ramasamy, M., Ramalingam, V., Natesan, K., Duraisamy, M., Venkatachalam, J., Shin, T., Seralathan, K.-K., 2021. Enhanced visible light-driven photocatalysis of iron-oxide/titania composite: Norfloxacin degradation mechanism and toxicity study. Journal of Hazardous Materials 412, 125330.

Monteagudo, J.M., Durán, A., Martín, I.S., García, S., 2014. Ultrasound-assisted homogeneous photocatalytic degradation of reactive blue 4 in aqueous solution. Applied Catalysis. B, Environmental 152–153, 59–67. https://doi.org/10.1016/j.apcatb.2014.01.014.

Oliveira, V.L., Lima, A.L.D., Gabriel, J.B., Pereira, M.C., Souza, T.S.F., Ardisson, J.D., Machado, A.R.T., Silva, A.C., 2020. Enhanced Photocatalytic Activity of TiO2/γ-Fe2O3 by Using H2O2 as an Electron Acceptor Under Visible Light Radiation. Water, Air, and Soil Pollution 231 (12). https://doi.org/10.1007/s11270-020-04916-0.

Rosa, D., D'Agostino, F., Bavasso, I., Bracciale, M.P., Di Palma, L., 2023a. Easy way to produce iron-doped titania nanoparticles via the solid-state method and

investigation their photocatalytic activity. Journal of Materials Research 38 (5), 1282–1292.

Rosa, D., Agostino, F.D., Bavasso, I., Di Palma, D., 2023b. An Innovative and Easy Method for Iron-doped Titania Synthesis. Chemical Engineering Transactions 101, p. https://doi.org/10.3303/CET23101003.

Rubio, D., Nebot, E., Casanueva, J.F., Pulgarin, C., 2013. Comparative effect of simulated solar light, UV, UV/H2O2 and photo-Fenton treatment (UV-Vis/H2O2/Fe2+,3+) in the Escherichia coli inactivation in artificial seawater. Water Research 47 (16), 6367–6379. https://doi.org/10.1016/j.watres.2013.08.006.

S. H U -S U N G L I N † A N D M I R A. "Catalytic Decomposition of Hydrogen Peroxide on Iron Oxide: Kinetics, Mechanism, and Implications," 1998. [Online]. Available: https://pubs.acs.org/sharingguidelines.

Santos, R.d.S., Faria, G.A., Giles, C., Leite, C.A.P., Barbosa, H.d.S., Arruda, M.A.Z., Longo, C., 2012. Iron insertion and hematite segregation on Fe-doped TiO 2 nanoparticles obtained from sol-gel and hydrothermal methods. ACS Applied Materials & Interfaces 4 (10), 5555–5561.

Subramaniam, M.N., Goh, P.S., Lau, W.J., Ismail, A.F., Karaman, M., 2020. Enhanced visible light photocatalytic degradation of organic pollutants by iron doped titania nanotubes synthesized via facile one-pot hydrothermal. Powder Technology 366, 96–106. https://doi.org/10.1016/j.powtec.2020.02.052.

Thomas, N., Dionysiou, D.D., Pillai, S.C., 2021. Heterogeneous Fenton catalysts: A review of recent advances. Journal of Hazardous Materials 404, 124082.

Uddin, M.J., Islam, M.A., Haque, S.A., Hasan, S., Amin, M.S.A., Rahman, M.M., 2012. "Preparation of nanostructured TiO2-based photocatalyst by controlling the calcining temperature and pH". Int Nano Lett 2 (1). https://doi.org/10.1186/2228-5326-2-19.

Wang, S., 2008. A Comparative study of Fenton and Fenton-like reaction kinetics in decolourisation of wastewater. Dyes and Pigments 76 (3), 714–720. https://doi.org/10.1016/j.dyepig.2007.01.012.

Wei, X., Li, J., Liu, Z., Yang, X., Naraginti, S., Xu, X., Wang, X., 2018. Visible light photocatalytic mineralization of 17α-ethinyl estradiol (EE2) and hydrogen evolution over silver and strontium modified TiO2 nanoparticles: Mechanisms and phytotoxicity assessment. RSC Advances 8 (8), 4329–4339.

Yegane Badi, M., Vosoughi, M., Sadeghi, H., Mokhtari, S.A., Mehralipour, J., 2022. Ultrasonic-assisted H2O2/TiO2 process in catechol degradation: kinetic, synergistic and optimisation via response surface methodology. International Journal of Environmental Analytical Chemistry 102 (3), 757–770. https://doi.org/10.1080/03067319.2020.1726335.

Yu, J., Xiang, Q., Zhou, M., 2009. Preparation, characterization and visible-light-driven photocatalytic activity of Fe-doped titania nanorods and first-principles study for electronic structures. Applied Catalysis. B, Environmental 90 (3–4), 595–602. https://doi.org/10.1016/j.apcatb.2009.04.021.

Zhang, Y., Wu, L., Wang, Y., Zhang, Y.i., Wang, H., Wang, X., Chen, X.D., Wu, Z., 2021. Highly dispersed titania-supported iron oxide catalysts for efficient heterogeneous photo-Fenton oxidation: Influencing factors, synergistic effects and mechanism insight. Journal of Colloid and Interface Science 587, 467–478.

Zuorro, A., Lavecchia, R., Monaco, M.M., Iervolino, G., Vaiano, V., 2019. Photocatalytic degradation of azo dye reactive violet 5 on fe-doped titania catalysts under visible light irradiation. Catalysts 9 (8), pp. https://doi.org/10.3390/catal9080645.